Bianchi *et al. J Artif Intell Smart Energy Syst* (2024) 3:42
https://doi.org/10.68159/v548334254

ORIGINAL RESEARCH **Open access**

Hybrid Fuzzy Sliding Mode Control of UPQC for Power Quality Improvement in Solar PV–Battery EV Charging Systems

Luca Bianchi[1*], Marco Rossi[1], Giulia Romano[2]

Abstract

The integration of renewable energy systems into the electrical grid, alongside advancements in power electronics used to manage nonlinear loads, has significantly influenced power quality (PQ). This research emphasizes the improvement of PQ in both grid-tied and isolated solar photovoltaic systems (SPVS) equipped with a battery energy storage device (BESD) to supply an electric vehicle (EV) charging station (EVCS) alongside conventional local loads. A novel hybrid control mechanism integrating the advantageous features of a sliding mode controller (SMC) and a fuzzy logic controller (FLC) is proposed for the shunt filter of a unified power quality conditioner (UPQC). The primary objective is to maintain a stable DC link voltage (SVDC) amidst fluctuations in solar irradiation and varying load conditions (including EVCS and both balanced and unbalanced nonlinear loads). Additionally, it aims to minimize the total harmonic distortion (THD) in the source current and load voltage, while effectively alleviating voltage sags, swells, and source unbalances. The performance of the proposed model is evaluated across two operational modes (grid-connected and islanded) through four distinct case studies featuring diverse load configurations and grid voltage conditions. To demonstrate the enhanced efficacy of the proposed technique, a comparative analysis is conducted against conventional approaches, specifically proportional integral controllers (PIC) and standalone SMCs. The proposed strategy successfully decreases the THD to 2.25 %, 2.36 %, and 1.71 %, yielding distortion levels that are lower than those of the existing techniques identified in the literature survey.

Keywords Fuzzy logic controller, Sliding mode controller, UPQC, Solar system, Battery storage system

*Correspondence:
Luca Bianchi
luca.bianchi@unimi.it
[1] Department of Artificial Intelligence for Energy Networks, Faculty of Engineering, University of Milan, Milan, Italy
[2] Department of Intelligent Electrical Engineering, Polytechnic University of Turin, Turin, Italy

Introduction

Power quality (PQ) anomalies can induce significant disruptions in grid-connected electrical equipment. For example, voltage sags, swells, harmonic distortions, fluctuations, and power outages may result in equipment malfunction, data corruption, or physical damage. Preserving high PQ is critical, particularly in highly sensitive settings such as medical facilities. Furthermore, utility providers must guarantee consistent and dependable power distribution to sustain optimal PQ for end-users. In addition, incorporating renewable energy sources into distribution networks represents a fundamental step toward a more sustainable and eco-friendly energy infrastructure.

Nevertheless, this integration introduces multiple operational difficulties owing to the unpredictable and fluctuating nature of renewable resources, such as solar and wind energy. Among all PQ challenges, total harmonic distortion (THD) remains the most critical priority. Minimized THD levels are highly desirable in electrical networks, as elevated THD can precipitate problems including thermal overloading in equipment, signal interference in communication networks, and

This is an open access article distributed under the terms of the Creative Commons Attribution-NonCommercial-ShareAlike 4.0 International License (CC BY-NC-SA 4.0), which permits non-commercial use, distribution, reproduction, and adaptation in any medium or format, provided that appropriate credit is given to the original author(s) and source, a link to the license is provided, and any changes made are indicated. Adapted material must be distributed under the same license.

© 2024 The Author(s). | Published by Institute of Smart Energy Systems Press

overall degradation of system efficiency. Consequently, securing PQ stability has emerged as a predominant focus for electrical engineers.

Literature review

The implementation of UPQC algorithms and control methodologies for PQ improvement offers an adaptable regulatory framework to boost overall system efficiency. The proposed dynamic control scheme demonstrates enhanced performance in evaluating the critical three-phase system under investigation [1]. By employing a unit vector control strategy, a single-phase UPQC is utilized in this study to execute grid-integrated photovoltaic tasks, including the mitigation of voltage sags and swells, unit power factor correction, and the elimination of voltage and current harmonics. A phase-locked loop (PLL) mechanism within the unit vector template control framework prevents significant zero-crossing errors when detecting highly corrupted supply voltages. Furthermore, the grid-tied PV UPQC relies on a PLL-based control architecture for its inverters [2].

This indicates that specific modifications are necessary to improve PQ further. The current investigation primarily focuses on the UPQC. Functioning both concurrently and independently, the UPQC mitigates voltage- and current-based distortions. By simultaneously compensating for harmonics and load current irregularities, the UPQC improves PQ by ensuring the source current and load voltage maintain a sinusoidal waveform at the required voltage magnitude [3]. Furthermore, by implementing the proposed control mechanism, reference DC link voltage regulation combined with an adaptive neuro-fuzzy inference system (ANFIS) for DC voltage estimation significantly augments the UPQC's compensatory capabilities. The online simulation employs an ANFIS model that was trained offline [4].

In addition, a Fourier transform method was developed for renewable energy sources and integrated with a BESD for the UPQC to minimize voltage fluctuations and current load irregularities [5]. The proposed model incorporated four distinct compensatory elements to improve the network's PQ. Flexible AC transmission systems (FACTS) compensators were evaluated within this framework. A real-time benchmark dataset was generated across various PQ scenarios. Based on this dataset, an intelligent deep learning controller model was formulated to regulate the system and guarantee a continuous, stable power supply [6]. The UPQC was selected to alleviate voltage distortions and current harmonics utilizing an ANFIS-based control strategy. Additionally, it boosts the effectiveness of the network [7]. The FLC was specifically designed for the SEAF to address and rectify voltage and current-related PQ issues in three-phase distribution networks [8].

An ant colony optimization (ACO) technique was introduced to optimize the Kp and Ki parameters of the PIC, aiming to minimize THD across diverse load configurations for the SHPF [9]. The designed system was analyzed using an ANFIS approach. The fuzzy controller improves system efficiency and facilitates the generation of current references by applying linguistic terminology to determine system parameters [10]. A highly adaptable FLC is scheduled to respond dynamically as system parameters fluctuate. The UPQC is subjected to both static and switching nonlinear loads, proving capable of eliminating harmonics while reducing voltage fluctuations, sags, and swells [11]. A Genetic Algorithm (GA)-optimized ANFIS controller was proposed to compensate for PQ disturbances and manage the system's DC link voltage (DLV). Consequently, this technique generates an optimal DC-link regulating voltage [12].

Within the proposed microgrid architecture, a robust UPQC—frequently paired with conventional power sources—is evaluated to regulate power flow. Its performance was further optimized through the application of the ANFIS methodology [13]. This study introduces an artificial neural network (ANN) control strategy for the UPQC based on the Levenberg-Marquardt Backpropagation (LMBP) algorithm. The proposed power distribution framework includes the LMBP, a back-to-back five-level diode-clamped converter (DCC), a three-phase three-wire distribution network, sinusoidal PWM, a hysteresis current controller, and power angle adjustment (PAA). Various abnormal fault conditions, such as single-phase-to-ground faults, are treated as highly complex analytical challenges. In this research, the ANN-based

© 2024 The Author(s). | Published by Institute of Smart Energy Systems Press

controller is designed to route power between converters without increasing the Voltage Source Converter (VSC) specifications, thereby reducing overall system expenses [14].

The multi-converter UPQC (MC-UPQC) employs two series VSCs to transmit power across feeders, effectively removing system transients, voltage sags, swells, and interruptions. By integrating a hybrid metaheuristic approach known as the beetle swarm-based butterfly optimization algorithm to optimize membership limits and generate control rules, the proposed model implements control schemes based on an optimized FLC within a synchronous reference frame technique. The primary advantage of this optimized FLC-based MC-UPQC is its rapid response in minimizing THD for both source and load-side voltages and currents [15]. Additionally, a novel hybrid algorithm combining the path finder algorithm and the grey wolf optimizer was designed to locate and size a UPQC to enhance PQ accurately. This model evaluates the voltage stability index, power loss, and UPQC installation budget to determine the optimal integration site [16].

Furthermore, a UPQC integrated with a superconducting magnetic energy storage (SMES) system for EVCS applications was developed to manage grid voltage anomalies and load current harmonics, which are common electrical disruptions that this UPQC-SMES setup effectively controls. To further protect the compromised grid, an advanced Vehicle-to-Grid (V2G)-based compensation strategy is suggested to address voltage swells and sags [17]. This study introduces a universal active power filter (UAPF) for microgrid configurations incorporating renewable energy. In this setup, the BSS and renewable energy sources, such as solar and wind, are coupled at the UAPF's DC-link. A centralized microgrid controller (CMC) is deployed to enhance PQ and efficiently regulate power flow within the suggested microgrid system. The primary objectives of the CMC include achieving optimal renewable energy utilization and ensuring uninterrupted power delivery to the load under diverse operational conditions [18].

To effectively address existing current and harmonic distortions, it is recommended to use a novel PIC that employs the Automatically Updating-Sparrow Search optimization. This controller has been successfully interfaced with clean energy sources, specifically wind turbine squirrel cage induction generators [19]. This investigation introduces an innovative heuristic-based adaptive control methodology designed to augment the UPQC's compensatory capabilities. Conventional fixed-gain PIC methods often cause an increased error between the measured and reference DC voltages during sag events. Ultimately, this leads to insufficient PQ distortion compensation at the point of common coupling. To elevate the system's compensation proficiency, the behavior of the adaptive control technique (ACT) is evaluated using both analytical and artificial intelligence approaches [20].

Contribution of the work

Nevertheless, a review of existing literature reveals that many studies have concentrated solely on isolated objectives. In contrast, this proposed research concurrently addresses multiple objectives by testing various load configurations—including EV charging—alongside solar irradiation fluctuations and both balanced and unbalanced supply voltage states, utilizing grid-connected and standalone operational modes as test scenarios. The key contributions of this manuscript are:

· A fuzzy sliding mode hybrid controller (FSMC) is proposed for the UPQC to manage EVCS loads in conjunction with the base load.

· The primary goals include reducing source current THD and regulating SVDC during fluctuations in both load and solar irradiation, alongside effective compensation of voltage sags, swells, and grid disturbances.

· The solar energy system (SES) and battery storage system (BSS) are interfaced with the UPQC's DC connector to stabilize the SVDC during load variations and to meet power demands while minimizing stress on the converters.

· The proposed controller's performance for the UPQC, integrated with SPVS and BESD systems, was analyzed across four distinct test cases within two operational modes (grid-tied and islanded). These evaluations encompassed

© 2024 The Author(s). | Published by Institute of Smart Energy Systems Press

various combinations of grid/island states, dynamic loads, solar irradiation variations with partial shading, and supply voltage imbalances.

· To validate the superiority of the proposed framework, a comparative analysis was performed against conventional control methodologies, specifically PIC and SMC, as well as additional controllers identified in the literature survey.

Proposed test system

The architecture of the developed photovoltaic-integrated UPQC is illustrated in **Figure 1**. The SPVS, alongside the BESD, is connected to the UPQC through a DC link that incorporates both a boost converter and a buck-boost converter. The UPQC itself is composed of a shunt active filter (SHAF) and a series active filter (SEAF). The primary function of the SEAF is to alleviate voltage variations by injecting the required compensation voltage. Additionally, a transformer establishes galvanic isolation between the voltage source converters (VSCs) and the utility grid. Conversely, the main purpose of the SHAF is to minimize imperfections in the current signals by supplying the requisite harmonic current (ISH) and ensuring a rapid response for SVDC regulation. A three-phase rectifier was selected to accommodate both balanced and unbalanced load conditions.

© 2024 The Author(s). | Published by Institute of Smart Energy Systems Press

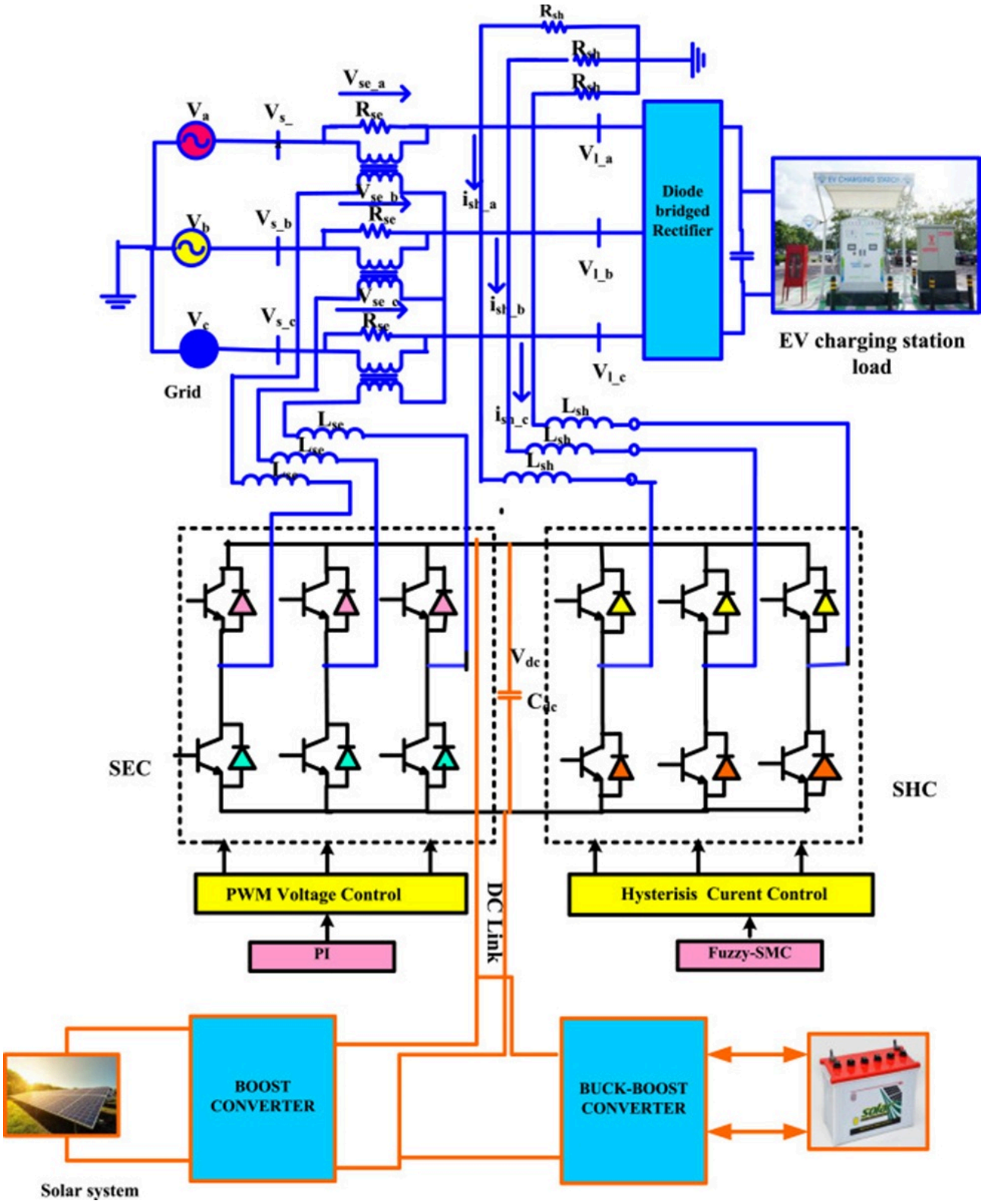


Figure 1. Structure of the proposed U-SEBES.

© 2024 The Author(s). | Published by Institute of Smart Energy Systems Press

Modelling of PV and battery components

Integrating solar and battery systems to power the DC link is suggested for the UPQC. The DC link capacitor voltage (DCLCV) is managed by a renewable energy source coupled with a battery storage system, providing support during shifts in power consumption. By reducing the burden on the main utility grid, these external power sources help lower the required converter ratings and minimize operational stress.

SPVS

The PV model utilized in this research was developed using the Simulink software suite. To achieve the necessary voltage level, PV modules are linked in series to form a string. Following this, multiple strings are arranged in parallel to produce the desired electrical current. As shown in **Figure 2,** each photovoltaic (PV) cell within the module is modeled using a simplified single-diode circuit diagram.

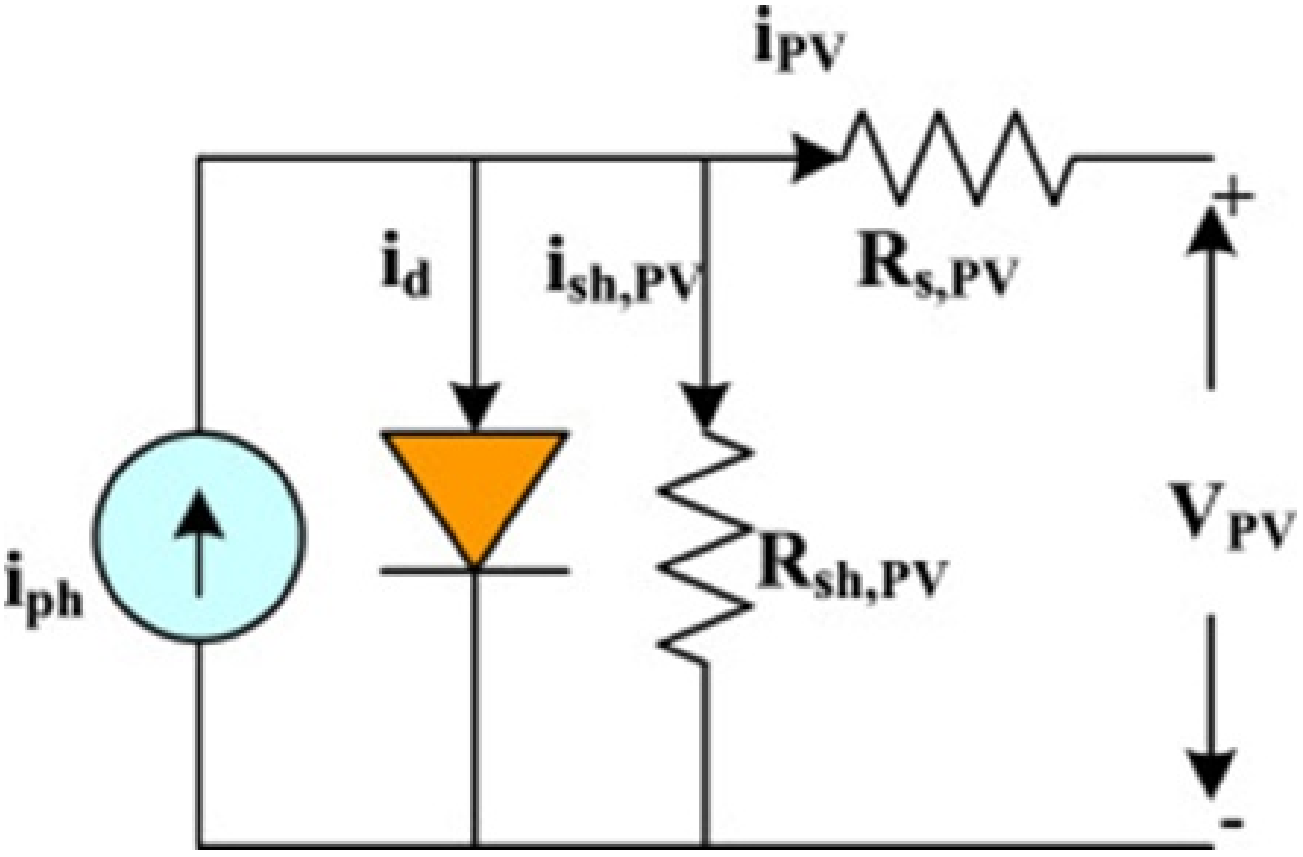


Figure 2. Equivalent model of PV cell.

This equivalent circuit comprises series and shunt resistors ($R_{s,PV}$, $R_{sh,PV}$) and a current source (i_{PV}, $i_{sh,PV}$) operating through a forward-biased diode (id). The PV cell captures photon-induced current (iph) from sunlight, subsequently converting it into electrical energy. **Eq. 1** demonstrates the application of Kirchhoff's Current Law (KCL) to determine the output current of the PV cell.

$$i_{PV} = i_{ph} - i_d - i_{sh} \quad (1)$$

Various configurations of PV modules constitute the overall array, as defined by **Eq. 2.**

© 2024 The Author(s). | Published by Institute of Smart Energy Systems Press

$$i_{PV,m} = i_{ph}N_p - i_{S,PV}N_p\left[\exp\left(\frac{Q\left(V_{PV} + N_s/N_p\left(i_{PV,m}R_{S,PV}\right)\right)}{N_s\eta kT_C}\right) - 1\right] - \frac{V_{PV,m} + N_s/N_p\left(i_{PV,m}R_{S,PV}\right)}{N_s/N_p\left(R_{sh,PV}\right)} \quad (2)$$

Where,

$$i_{ph} = \left(i_{ph,n} + K_1\Delta T_C\right)\frac{G}{G_n} \quad (3)$$

In these expressions, the subscript “m” indicates the module; Np and Ns represent the count of parallel- and series-connected cells, respectively; G denotes solar irradiance; and T signifies temperature.

This study implements the Incremental Conductance maximum power point tracking (MPPT) technique, extracting the peak power output according to **Eq. 4.**

$$P_{PV} = V_{PV} \times i_{PV} \quad (4)$$

Here, VPV and PPV stand for the output voltage and power generated by the PV system, respectively.

The Incremental Conductance Method (ICM) is a widely recognized MPPT algorithm applied within photovoltaic setups. The fundamental objective of any MPPT algorithm is to maintain the PV system’s operation at its maximum power point (MPP), thereby optimizing power generation. The ICM accomplishes this by dynamically shifting the system’s operating point in response to environmental fluctuations, guaranteeing maximum energy extraction. This procedure relies on the solar panel’s incremental conductance (ΔI/ΔV), with ΔI representing the variation in current and ΔV denoting the variation in voltage. By evaluating this incremental conductance against a baseline reference, the algorithm dictates the necessary directional adjustment for the operating point. The operational flowchart for the ICM is depicted in **Figure 3.**

ICM is distinguished for its rapid and precise tracking capabilities under highly variable environmental circumstances, including sudden shifts in temperature and solar irradiance. Nevertheless, specific conditions may cause the algorithm to oscillate near the MPP. These oscillations can be mitigated by introducing hysteresis or integrating supplementary control techniques. Ultimately, while various MPPT algorithms present unique strengths and drawbacks, the selection of an appropriate method is contingent upon specific criteria, including performance demands, budget, and overall system complexity.

BESD

The energy storage system (ESS) utilizes a lithium-ion battery, which offers numerous advantages such as a low self-discharge rate and reduced maintenance requirements. Charging and discharging operations for the battery are controlled using switches SW1 and SW2, as illustrated in **Figure 4a.** The state-of-charge of the battery (SOCB) is mathematically expressed in **Eq. 5.**

$$SOCB = 60\left(1 + \int i_{BS}\, dtQ\right) \quad (5)$$

The decision to charge or discharge the battery depends on the power supplied by the SPS and WPGS, constrained by the SOCB limits outlined in **Eq. 6.**

$$SOCB_{\min} \leq SOCB \leq SOCB_{\max} \quad (6)$$

© 2024 The Author(s). | Published by Institute of Smart Energy Systems Press

In this context, Q, iB, and irefB signify the battery's charge, its measured current, and its reference current, respectively. Meanwhile, SOC max and SOC min define the maximum and minimum permissible boundaries for the SOCB. The variables "VB", "CB", and "LB" correspond to the voltage, capacitance, and inductance of the battery. Finally, Vdc and its reference denote the measured and target DC link capacitor voltages. The control schematic governing battery function relative to the desired DC link voltage is presented in **Figure 4b**. **Table 1** details the operational modes of the designed system. In contrast, **Table 2** enumerates the specific SPS and BESD parameters selected for this study.

Table 1. Modes of operation.

Mode	Action taken
Mode-1: When the grid is connected	The grid provides power to the load (EV), supported by SPS and BESD
Mode-2: During standalone condition	The SPS and BESD supply power directly to the load (EV)

Table 2. Literature review.

Reference number	Controller adopted	THD	DLCV balancing	Supply voltage sag, swell	Supply voltage disturbance	Nonlinear sensitive load	Unbalanced load	EV
[11]	FLC	✓			✓			
[12]	ANFIS	✓		✓	✓	✓	✓	
[13]	ANFIS	✓	✓	✓	✓	✓		
[14]	NNC	✓		✓	✓	✓		
[17]	PIC	✓		✓	✓	✓	✓	✓
[19]	PIC with sparrow search algorithm	✓		✓	✓			
[20]	ANFIS-PI	✓		✓	✓	✓	✓	
Proposed UPQC with FLC and SMC control system	FLC-SMC	✓	✓	✓	✓	✓	✓	✓

Shunt Converter

The primary purpose of the SHAF is to diminish waveform imperfections by injecting a suitable compensation current while simultaneously keeping the SVDC stable. The operational framework executes (i) coordinate transformations between abc and dq0 reference frames, and (ii) employs the FSMC to fulfill the desired control objectives. The control architecture for the SHAF, incorporating the proposed methodology, is illustrated in **Figure 5**. Given that the

© 2024 The Author(s). | Published by Institute of Smart Energy Systems Press

transformation processes between abc and dq0 frames have been extensively documented in the literature review, the subsequent sections will exclusively detail the control strategy of the proposed FSMC.

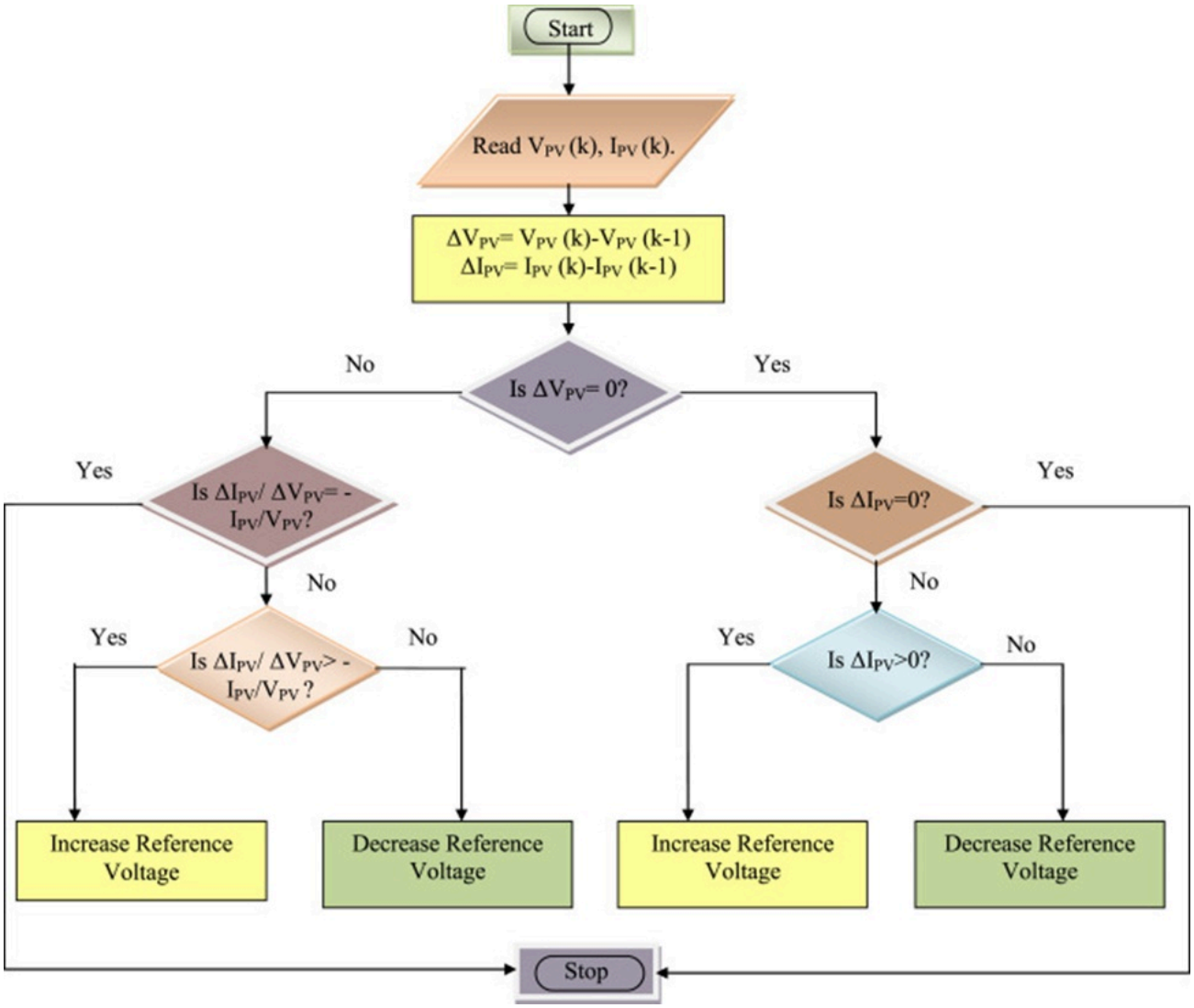
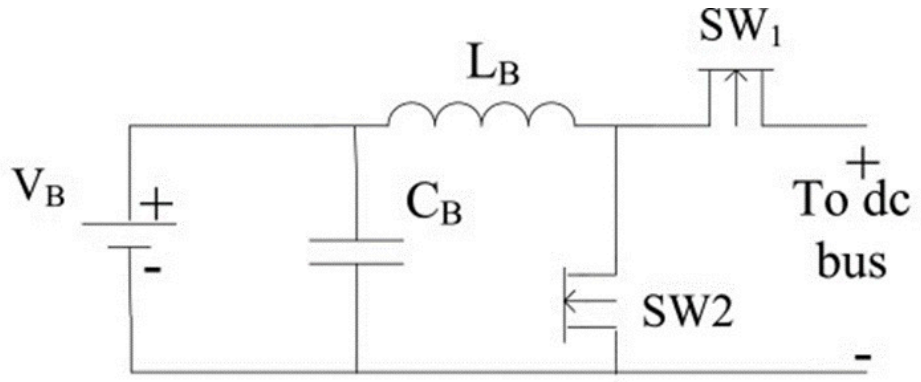
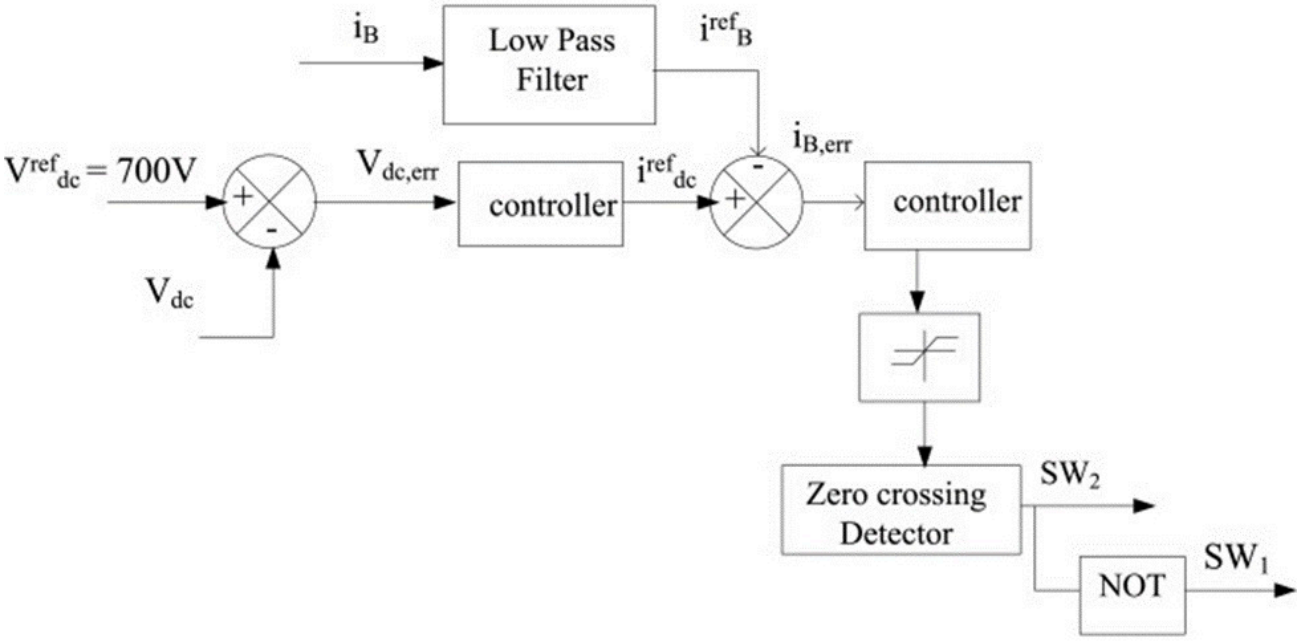


Figure 3. Flow chart of ICM-based MPPT.

© 2024 The Author(s). | Published by Institute of Smart Energy Systems Press



(a) ESS configuration at DC link



(b) ESS controller

Figure 4. ESS control.

© 2024 The Author(s). | Published by Institute of Smart Energy Systems Press

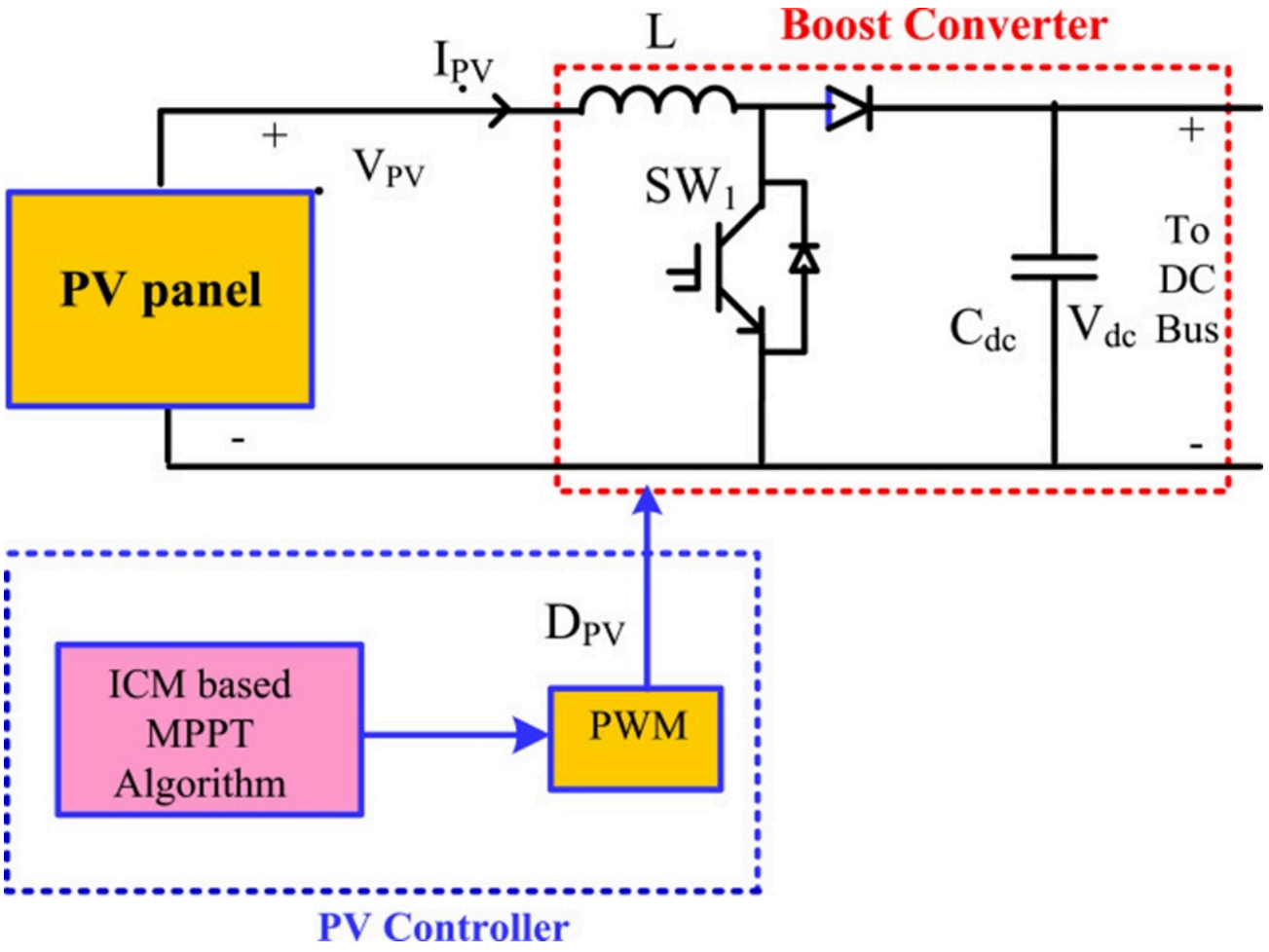
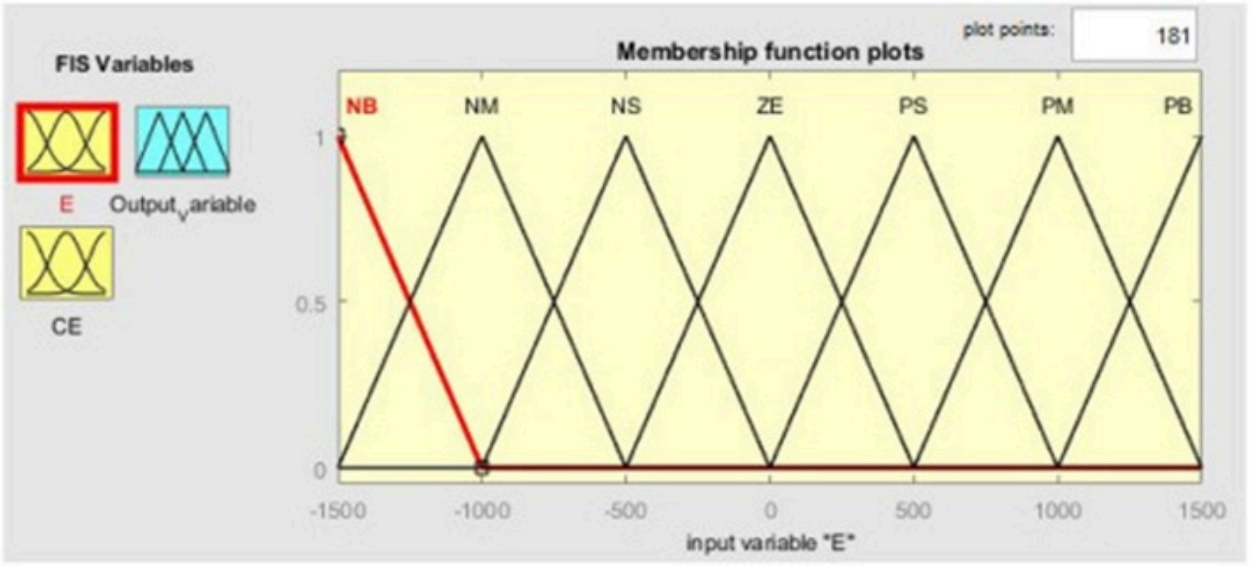


Figure 5. PV circuit.

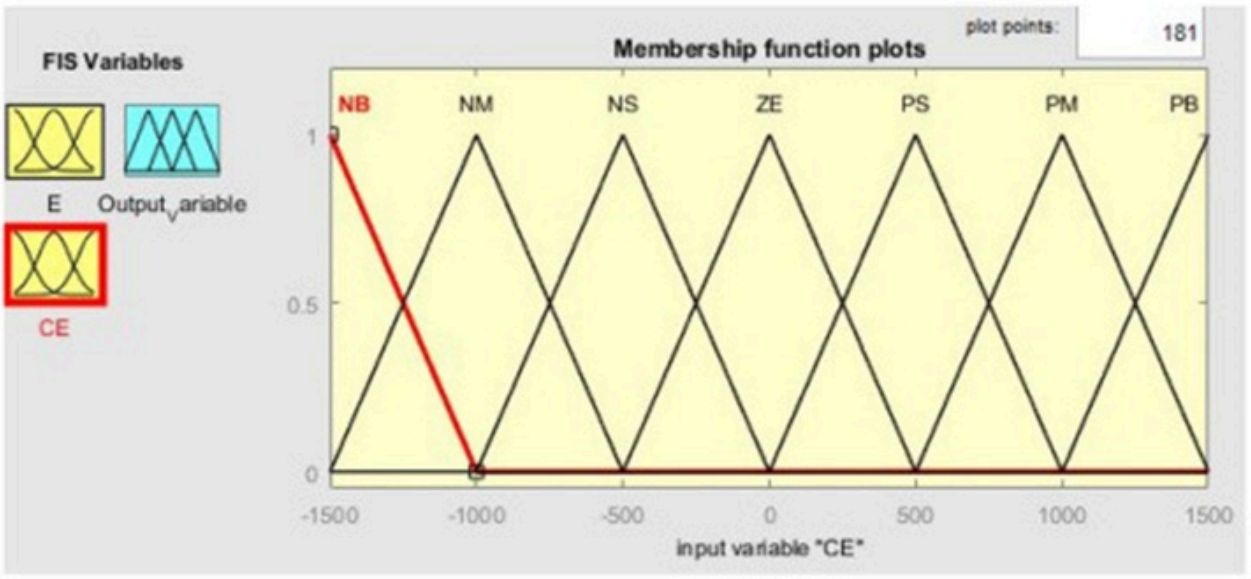
FSMC for SVDC

To regulate the DC link capacitor voltage, a fuzzy logic controller (FLC) acts as the primary regulator. This FLC takes the voltage error (E) and the rate of change of that error (CE) as input variables, producing a duty cycle (D) as its control output. Triangular membership functions map the error, change in error, and duty cycle, which are visually presented in **Figures 6a–6c,** respectively. The controller utilizes linguistic variables defined as ‘PB’ (Positive Big), ‘PM’ (Positive Medium), ‘PS’ (Positive Small), ‘ZO’ (Zero), and ‘NS’ (Negative Small). Additional classifications include ‘NM’ (Negative Small), ‘NM’ (Negative Medium) and ‘NB’ (Negative Big). The formulation of fuzzy “IF-THEN” rules relies on these linguistic parameters, which are tabulated in **Table 3**. While increasing the quantity of fuzzy rules can improve regulatory precision, it simultaneously increases the computational complexity of the system.

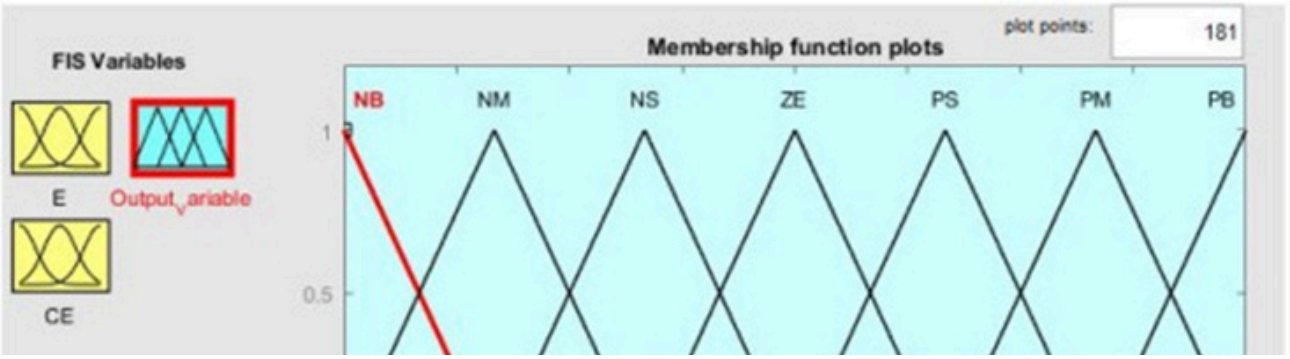
© 2024 The Author(s). | Published by Institute of Smart Energy Systems Press



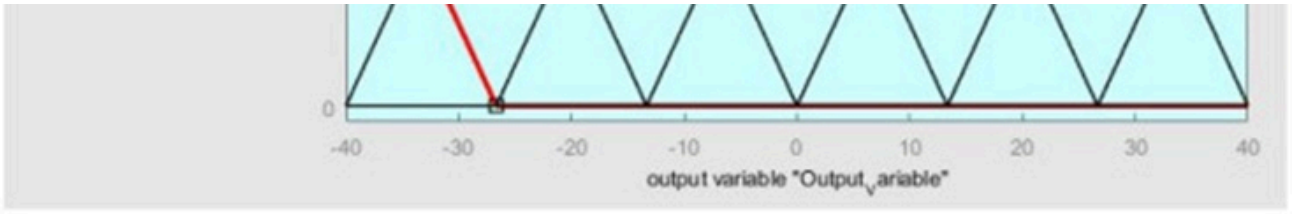
(a) E



(b) CE



© 2024 The Author(s). | Published by Institute of Smart Energy Systems Press



(c) O

NM	PS	ZE	NS	NM	NB	NB	NB
NS	PM	PS	ZE	NS	NM	NB	NB
ZE	PB	PM	PS	ZE	NS	NM	NB
PS	PB	PB	PM	PS	ZE	NS	NM
PM	PB	PB	PB	PM	PS	ZE	NS
PB	PB	PB	PB	PB	PM	PS	ZE

The sliding mode controller (SMC) is a robust nonlinear control strategy frequently applied across diverse engineering fields. Categorized as a variable structure control, it partitions system dynamics into distinct modes. It formulates a control law that compels the system's trajectory to align with a predefined switching surface, effectively "sliding" along it. The central objective of SMC is to confine the system state to this sliding surface, thereby guaranteeing resilience against external perturbations and parametric fluctuations. The fundamental steps involved in designing an SMC include: 1) formulating an appropriate sliding surface, 2) verifying the reachability of this surface, and 3) performing a rigorous stability analysis. The tracking error is computed according to **Eq. 7.**

$$x_1 = V^{ref}_{dc} - V_{dc} = e(n) \quad (7)$$

The corresponding derivatives of this calculated error are evaluated via **Eq. 8.**

$$x_2 = \frac{1}{T}e(n) - e(n-1) \quad (8)$$

Here, "T" signifies the time duration, whereas "x1" and "x2" act as the state-space variables. The mathematical expression defining their interrelationship is provided in **Eq. 9.**

$$\dot{x} = \begin{bmatrix} \dot{x_1} \\ \dot{x_2} \end{bmatrix} = \begin{bmatrix} 0 & 1 \\ 0 & 0 \end{bmatrix} \begin{bmatrix} x_1 \\ x_2 \end{bmatrix} + \begin{bmatrix} 0 \\ -k \end{bmatrix} \mu \quad (9)$$

Eqs. 10 and 11 establish the state-space representation of the designed sliding surface. **Eqs. 10 and 11**, respectively.

$$s = \begin{bmatrix} C & 1 \end{bmatrix} \begin{bmatrix} x_1 \\ x_2 \end{bmatrix} = Cx_1 + x_2 \quad (10)$$

© 2024 The Author(s). | Published by Institute of Smart Energy Systems Press

$$\dot{s} = [C \quad 1] \begin{bmatrix} \dot{x_1} \\ \dot{x_2} \end{bmatrix} = C\dot{x_1} + \dot{x_2} \quad (11)$$

The reaching power law for the controller is formulated as:

$$\dot{s} = -L|s|^{\alpha}\mathrm{sgn}(s) \quad (12)$$

Consequently,

$$\mathrm{sgn}(s) = \left\{ \begin{matrix} 1 \\ -1 \end{matrix} \right\} for \begin{matrix} s > 0 \\ s < 0 \end{matrix} \quad (13)$$

The parameter μ is derived using **Eq. 14.**

$$\mu = \frac{1}{K}[Cx_2 + L|s|^{\alpha}\mathrm{sgn}(s)] \quad (14)$$

The measured current is transformed into the dq synchronous reference frame utilizing phasor concepts, while a Phase-Locked Loop (PLL) synchronizes the frequency with the supply voltage. The effectiveness of the SHAF relies heavily on accurate reference current generation and precise management of the actual DC link voltage (VADLC). However, variations in the load demand can alter the system's power flow, subsequently causing the VADLC to fluctuate. Consequently, to maintain optimal stability of the VADLC, the active power managed by the SHAF must precisely compensate for internal switching losses. The proposed FSMC generates a DC error signal by comparing the measured DC link voltage against its reference setpoint, as established in **Eq. 15.**

$$\Delta i_{dc} = e_1(t) = V^{ref}{}_{dc} - V_{dc}(t) \quad (15)$$

This computed error signal from the FSMC is subsequently superimposed onto the d-axis component of the load-side current. To generate the necessary switching pulses, these dq-frame signals are inversely transformed back into the phasor frame. They are then compared against the actual load-side currents within a hysteresis current controller. The complete architecture of the proposed controller is depicted in **Figure 7.**

In this diagram, V_{s_abc} and V_{l_abc} correspond to the source and load voltages, respectively. The terms i_{l_dq0} and V_{s_dq0} represent the load currents and source voltages transformed into the dq0 reference frame. Finally, i_{sh_abc}, alongside V_{se_abc}, denote the injected compensation currents, voltages, and their corresponding reference values.

© 2024 The Author(s). | Published by Institute of Smart Energy Systems Press

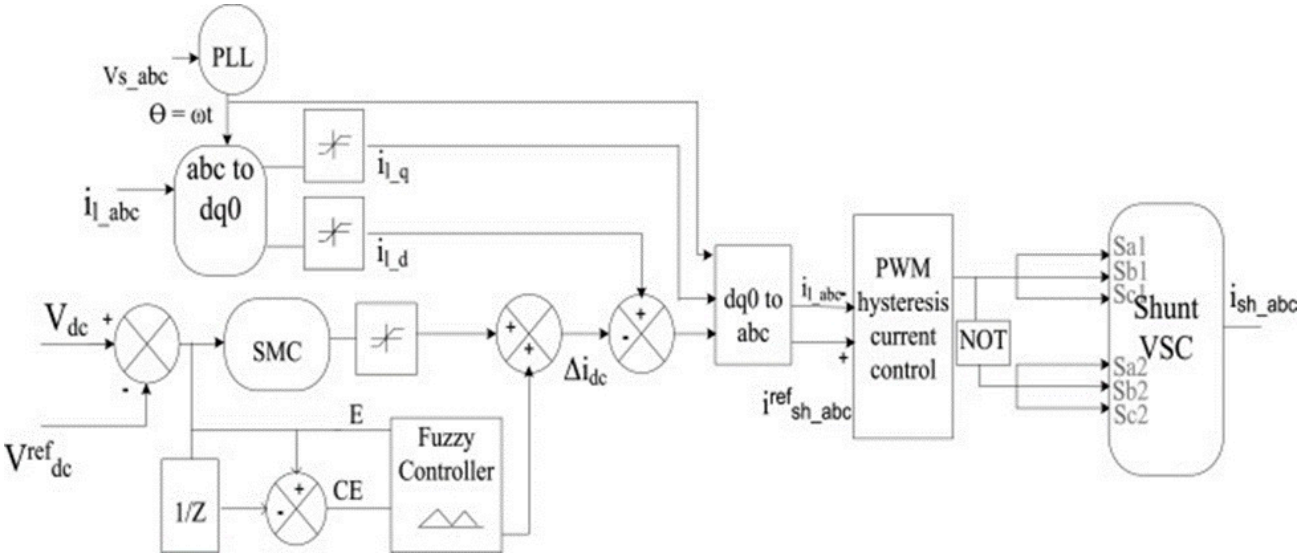


Figure 7. Hybrid Controller for Shunt Converter.

Series Controller

This controller generates operational signals by comparing the transformed load voltage against a designated reference voltage. Subsequently, this signal undergoes another frame transformation, as illustrated in **Figure 6**. A pulse-width modulation (PWM) controller is utilized to generate the necessary gating pulses. The control architecture for the series converter is presented in **Figure 8.**

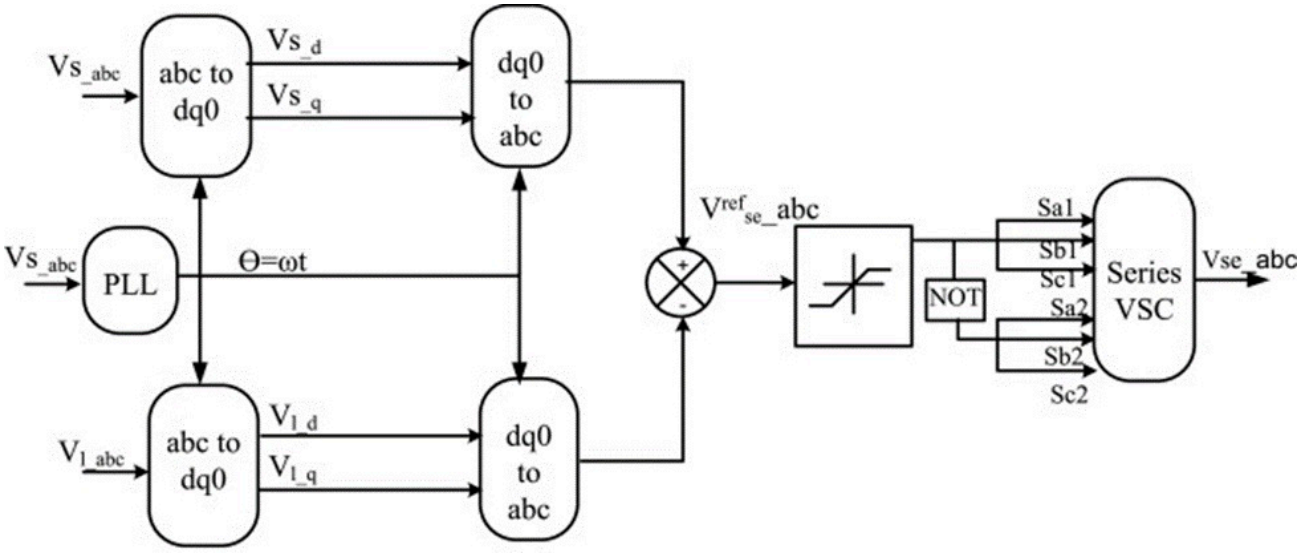


Figure 8. Series converter control system

Results and Discussion

A three-phase system was selected to verify the efficacy of the proposed hybrid controller. The designed methodology was modeled and simulated using MATLAB 2016 software. The enhanced capability of the developed FSMC-based UPQC is validated across two distinct operational scenarios (grid-tied and islanded modes) through four specific test studies. The first three cases are evaluated under scenario-1, while the fourth case falls under scenario-2. These

© 2024 The Author(s). | Published by Institute of Smart Energy Systems Press

evaluations encompass various configurations of nonlinear balanced and unbalanced loads, diverse source voltage conditions, and power quality (PQ) anomalies such as voltage sags, swells, and transient disturbances, all tested under both constant and fluctuating solar array irradiation. For test studies 1, 2, and 3, the source voltage is assumed to be balanced, whereas case 4 examines an unbalanced source voltage condition.

Furthermore, the total harmonic distortion (THD) for every case study was computed using **Eq. 16.** These outcomes were subsequently benchmarked against conventional PIC and SMC methods, along with other controllers identified in the literature survey, as detailed in **Table 4.**

$$THD = \frac{\sqrt{\sum_{n=1}^{N} I^2_n}}{I_f} \quad (16)$$

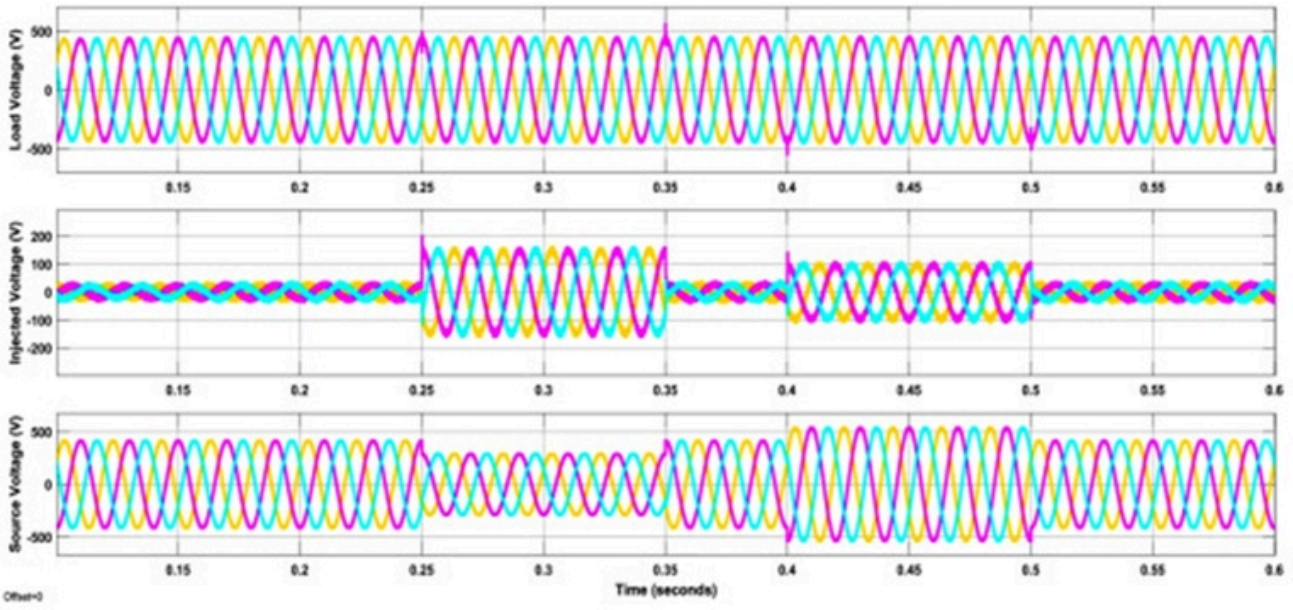
Table 4. Test cases considered.

Condition/Load	Test study1	Test study2	Test study3	Test study4
	Scenario-1 (Grid connected)			Scenario-2 (standalone)
Load 1 (Rectifier)	✓		✓	✓
Load 2 (p & q)		✓		
Load 3 (unbalanced L)			✓	
Load 4 (EV)	✓	✓	✓	✓
Fixed irradiation	✓			✓
Variable irradiation		✓	✓	
Supply voltage with balance	✓	✓		✓
Supply voltage with unbalance			✓	
Supply voltage Sag/swell	✓			
Supply voltage Disturbance		✓		
THD	✓	✓	✓	

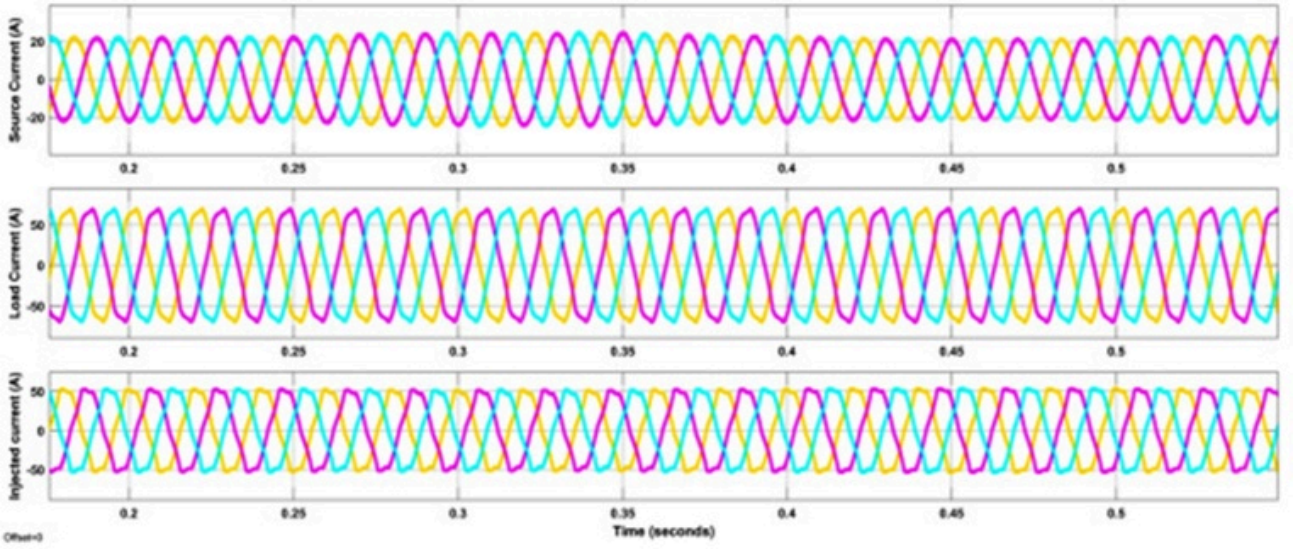
Here, In represents the nth-order harmonic component, while If denotes the fundamental component of the signal.

As illustrated in **Figure 9a** for the first test study under scenario-1, the supply voltage (VS) was considered balanced but subjected to a 30% sag and subsequent swell during the time intervals of 0.25–0.35 s and 0.4–0.5 s, respectively. In response, the solar- and battery-integrated UPQC identifies these voltage deviations, injects the appropriate series compensation voltage (Vse), and maintains a steady voltage at the load terminals. To evaluate the SHAF's performance, a three-phase balanced nonlinear load driven by a rectifier was utilized in conjunction with an EV charging station. According to **Figure 9b**, the current at the load terminals remained balanced but exhibited a non-sinusoidal profile. By mitigating these current signal imperfections, the proposed methodology successfully lowers the THD. Moreover, the current THD was minimized to 2.25%, a value significantly lower than those achieved by alternative methods documented in the research survey, such as PIC (approximately 3.8% and 14.7%), ANFIS (around 6.30%), and FLC (roughly 3.65%), as outlined in **Table 5** [reference number provided]. Additionally, as depicted in **Figure 9c**, the DC link voltage (VADLC) successfully stabilized at 700 V in under 0.05 s.

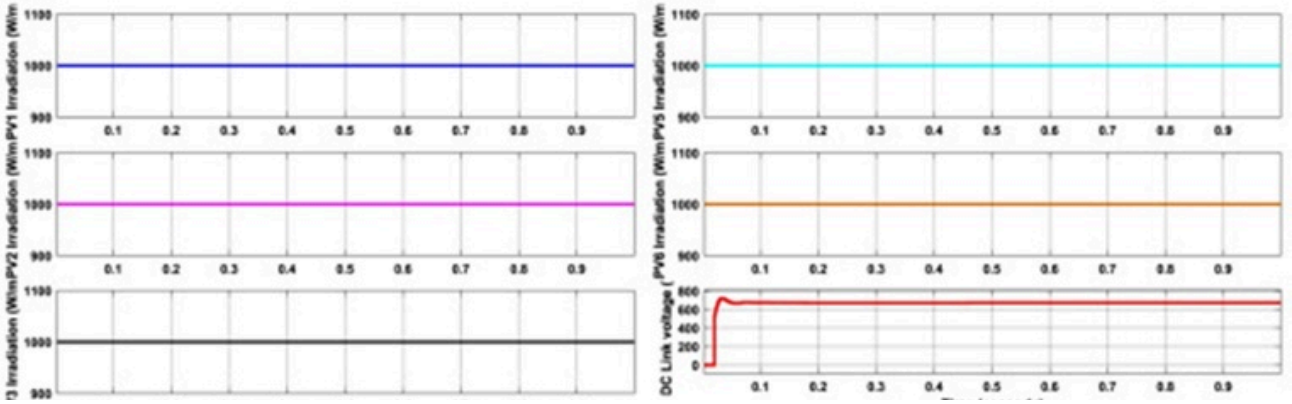
© 2024 The Author(s). | Published by Institute of Smart Energy Systems Press



(a) V_S, V_{se}, V_l



(b) i_l, i_{sh}, i_S



© 2024 The Author(s). | Published by Institute of Smart Energy Systems Press



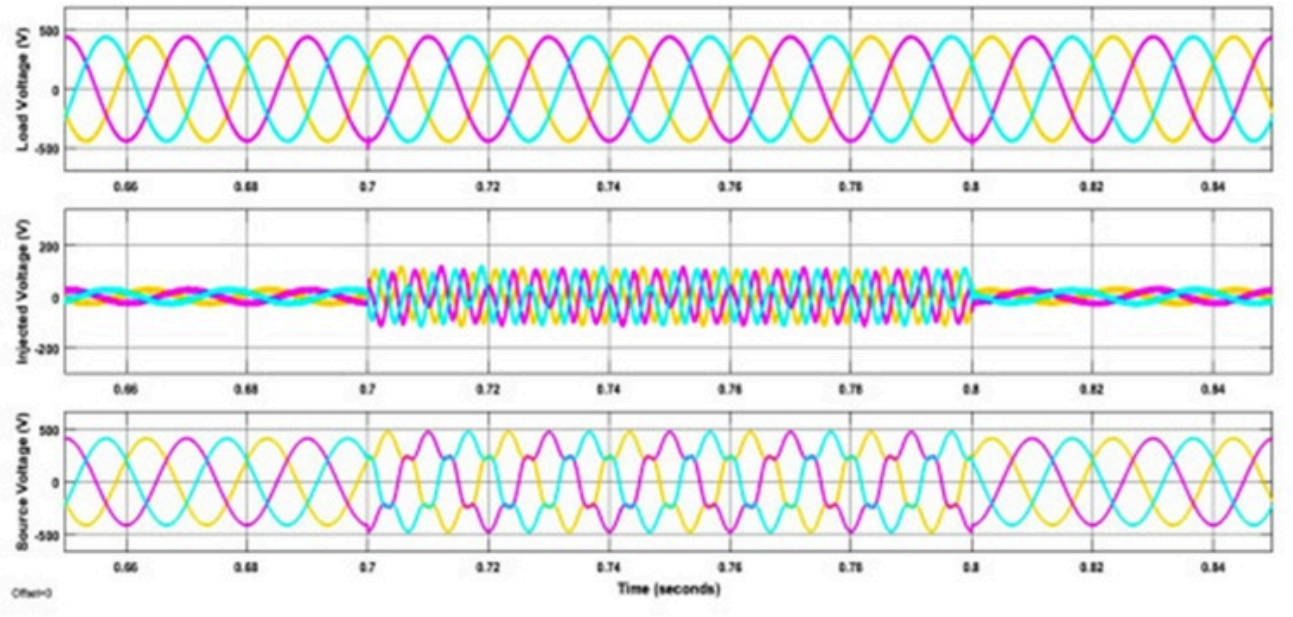
(c) G, SDCV

PIC	V_L	3.32	3.05	3.78	2.41	2.37	2.05	2.10	2.71	2.82
	I_S	5.12	4.99	5.31	4.36	4.97	5.02	4.8	4.6	5.1
SMC	V_L	3.44	3.16	3.01	2.39	2.37	2.52	2.25	2.62	2.22
	I_S	4.92	3.92	3.65	4.26	3.99	4.16	4.74	4.52	4.97
PIC[9]	V_L	–	–	–	–	–	–	–	–	–
	I_S	–	–	–	–	–	–	3.8	–	–
PIC[5]	V_L	–	–	–	–	–	–	–	–	–
	I_S	–	–	–	–	–	–	3.4	–	–
PIC[7]	V_L	–	–	–	–	–	–	–	–	–
	I_S	–	–	–	–	–	–	14.7	–	–
ANFIS[7]	V_L	–	–	–	–	–	–	–	–	–
	I_S	–	–	–	–	–	–	6.1	–	–
PIC[8]	V_L	–	–	–	–	–	–	–	–	–
	I_S	–	–	–	–	–	–	2.4	–	–
FLC[8]	V_L	–	–	–	–	–	–	–	–	–
	I_S	–	–	–	–	–	–	3.6	–	–
FSMC	V_L	**2.08**	**2.08**	**2.07**	**2.28**	**2.31**	**2.32**	**2.27**	**2.31**	**2.33**
	I_S	**1.71**	**1.78**	**2.27**	**2.36**	**2.54**	**3.06**	**2.25**	**2.39**	**2.95**

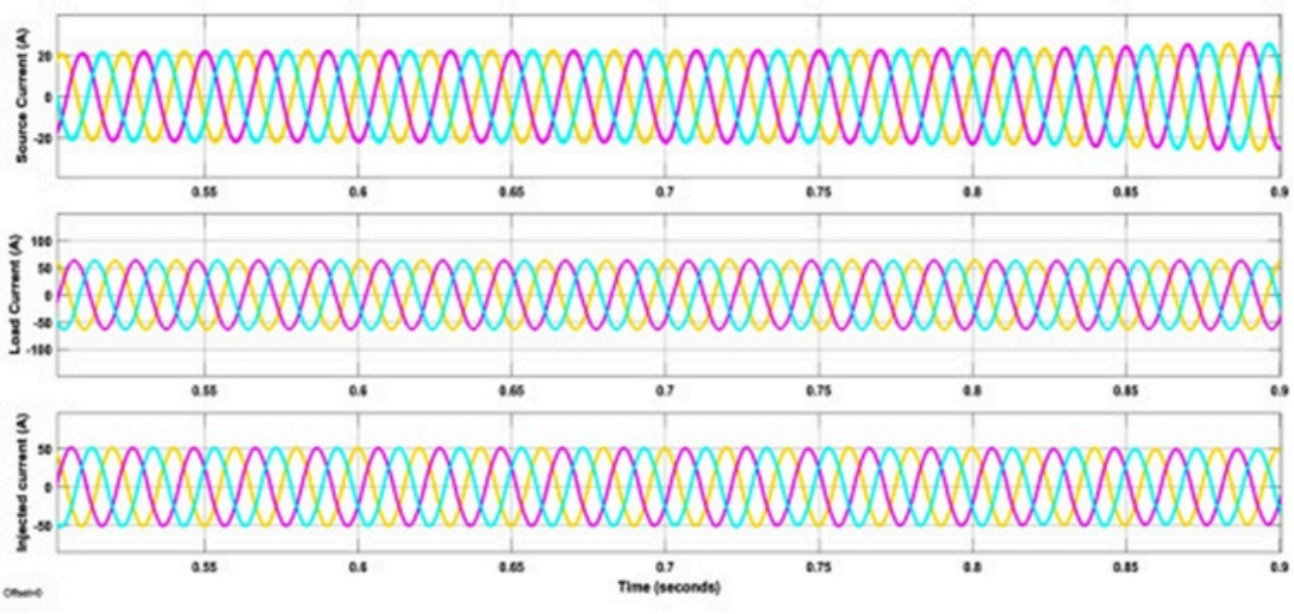
*Note: a, b, c are phases.

For case 2, a balanced VS was applied similarly to case 1. However, it included specific voltage aberrations as depicted in **Figure 10a**. The implemented strategy successfully preserved a constant voltage across the load terminals. Due to the integration of a linear balanced active-reactive power load alongside the EV charging station load, the measured load current was phase-balanced and sinusoidal, as demonstrated in **Figure 10b**. The proposed technique successfully curtailed the THD to 2.36%. This clearly indicates that the developed solution proficiently resolves both current- and voltage-related PQ challenges. Furthermore, **Figure 10c** illustrates the controller's robust capability to stabilize the DC link voltage at 700 V within a brief period of 0.02 s, even when subjected to concurrent changes in solar irradiation and load demand.

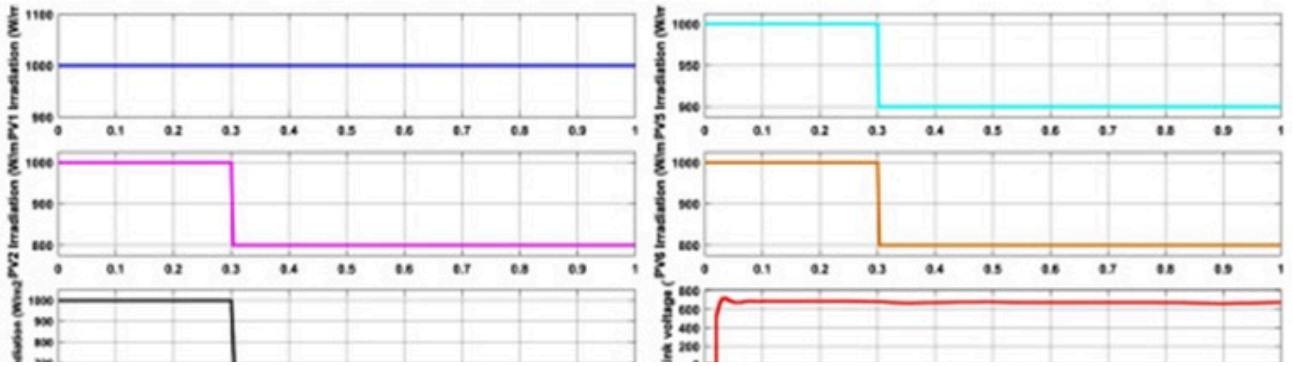
© 2024 The Author(s). | Published by Institute of Smart Energy Systems Press



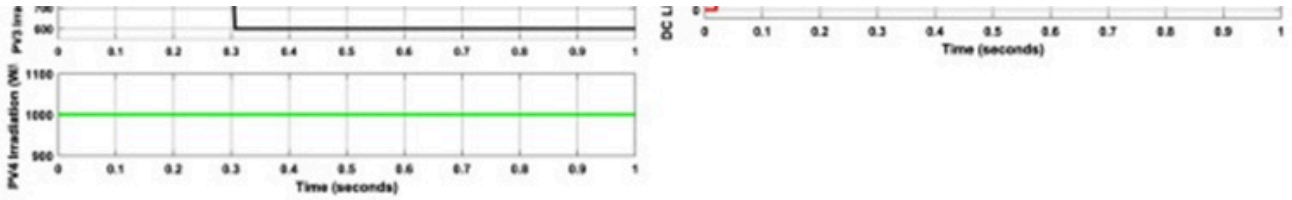
(a) V_S, V_{se}, V_l



(b) i_l, i_{sh}, i_S

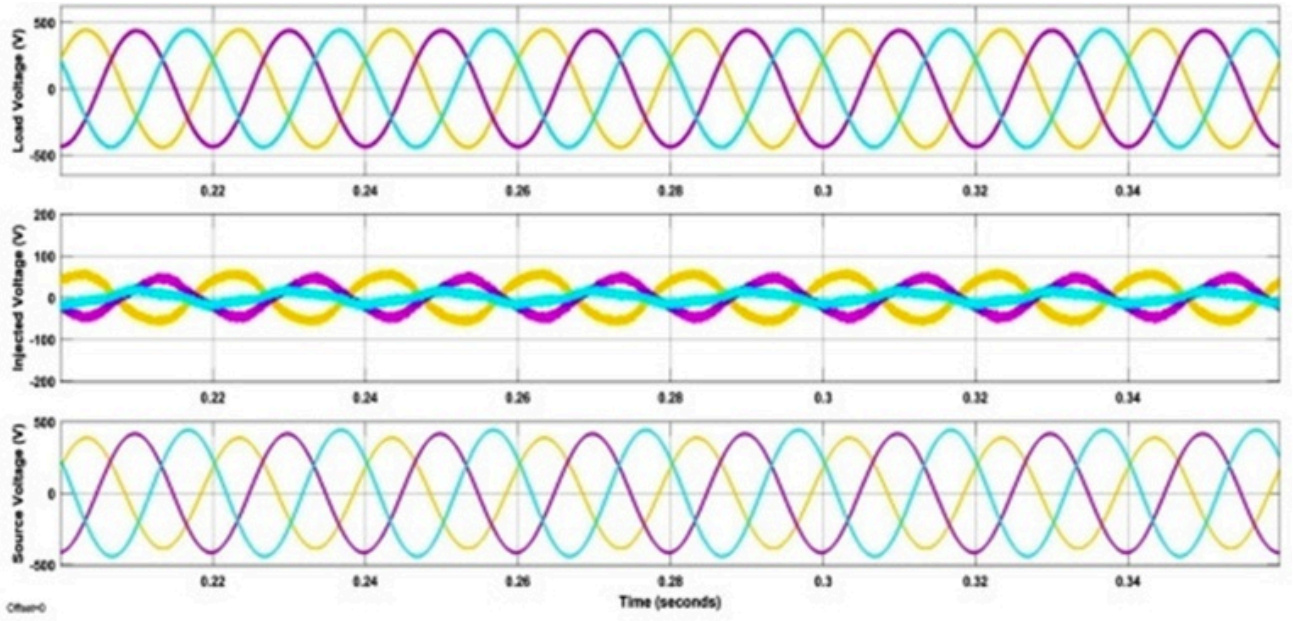


© 2024 The Author(s). | Published by Institute of Smart Energy Systems Press

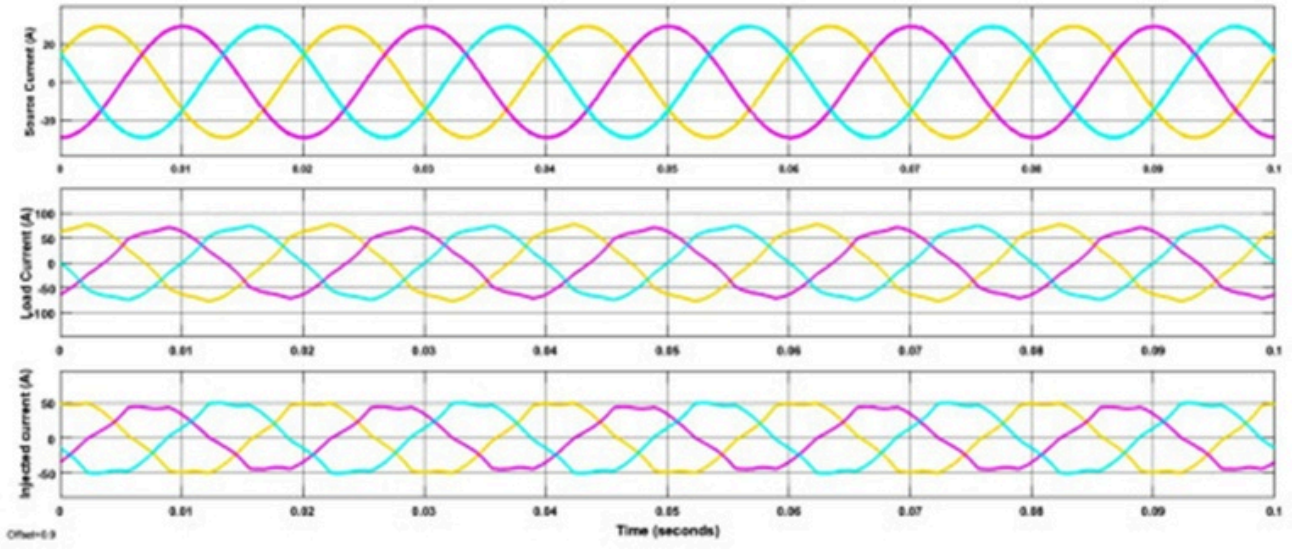


(c) G, SDCV

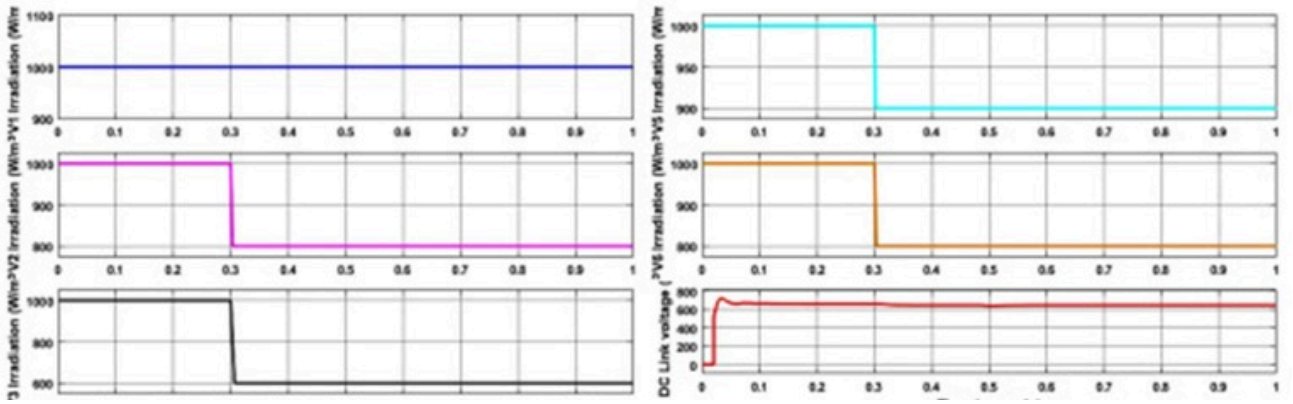
© 2024 The Author(s). | Published by Institute of Smart Energy Systems Press



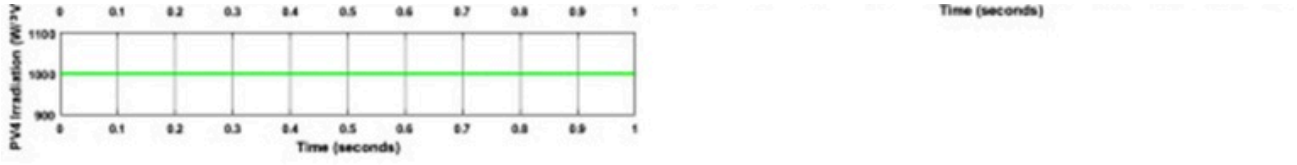
(a) V_S, V_{se}, V_l



(b) i_l, i_{sh}, i_S



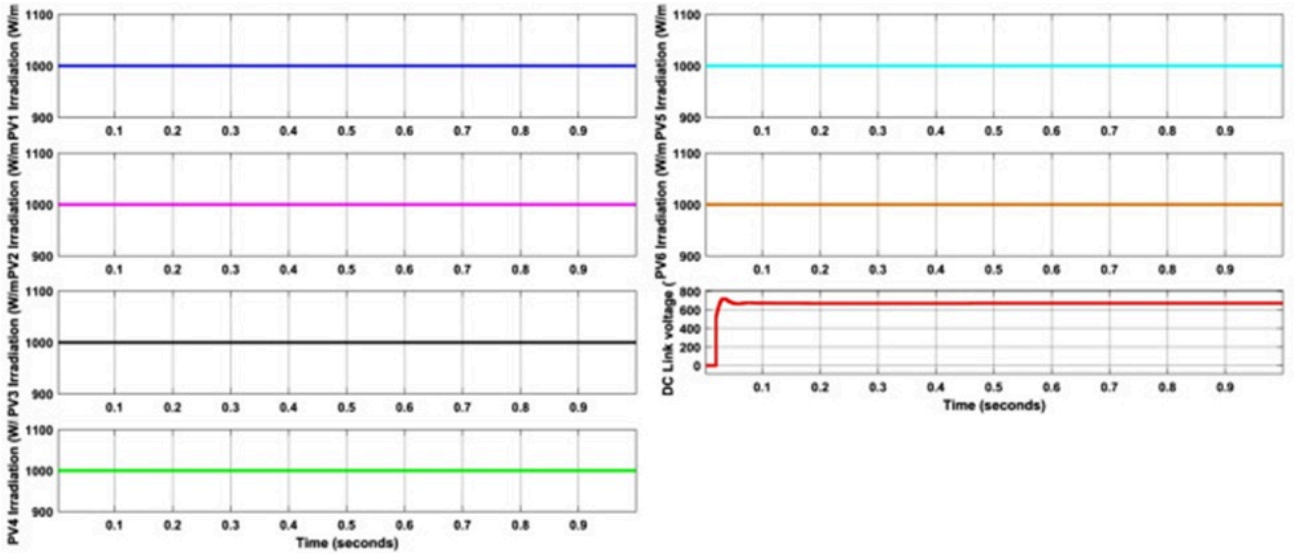
© 2024 The Author(s). | Published by Institute of Smart Energy Systems Press



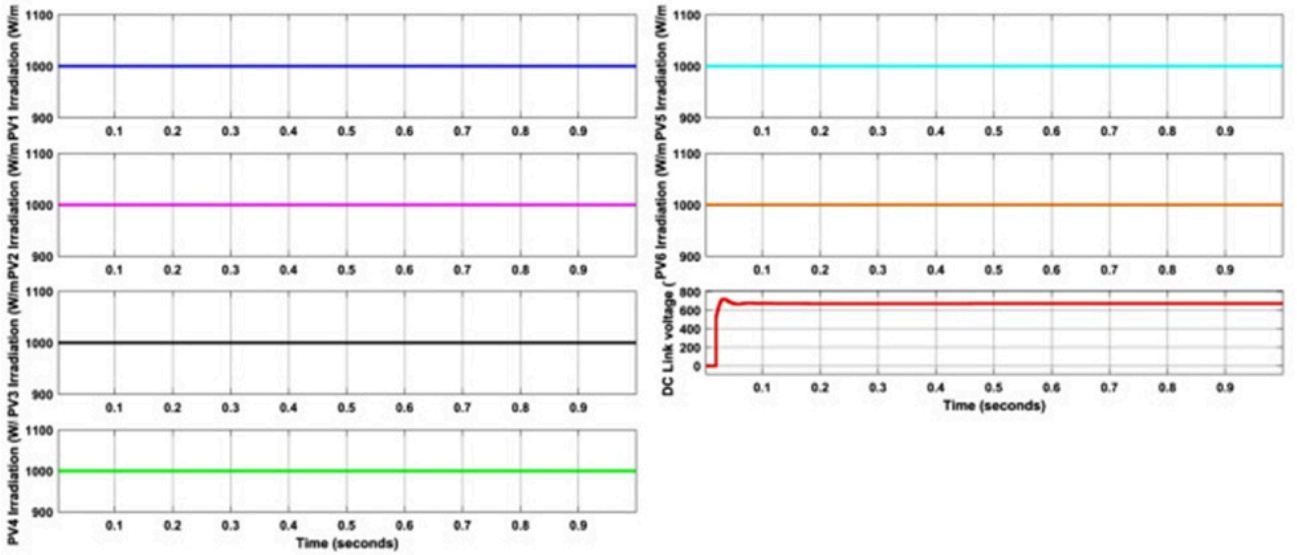
(c) G, SDCV

further evidenced in Figure 12c.

The frequency spectrum generated by the developed method across all experimental tests is displayed in **Figure 13**. Furthermore, **Figure 14** clearly shows that the required time (in seconds) for the DC link voltage to reach stability using the proposed method is substantially shorter than that of traditional approaches.



(b) G, DC Link Voltage



(b) G, DC Link Voltage

© 2024 The Author(s). | Published by Institute of Smart Energy Systems Press

Figure 12. U-SEBES for case-4

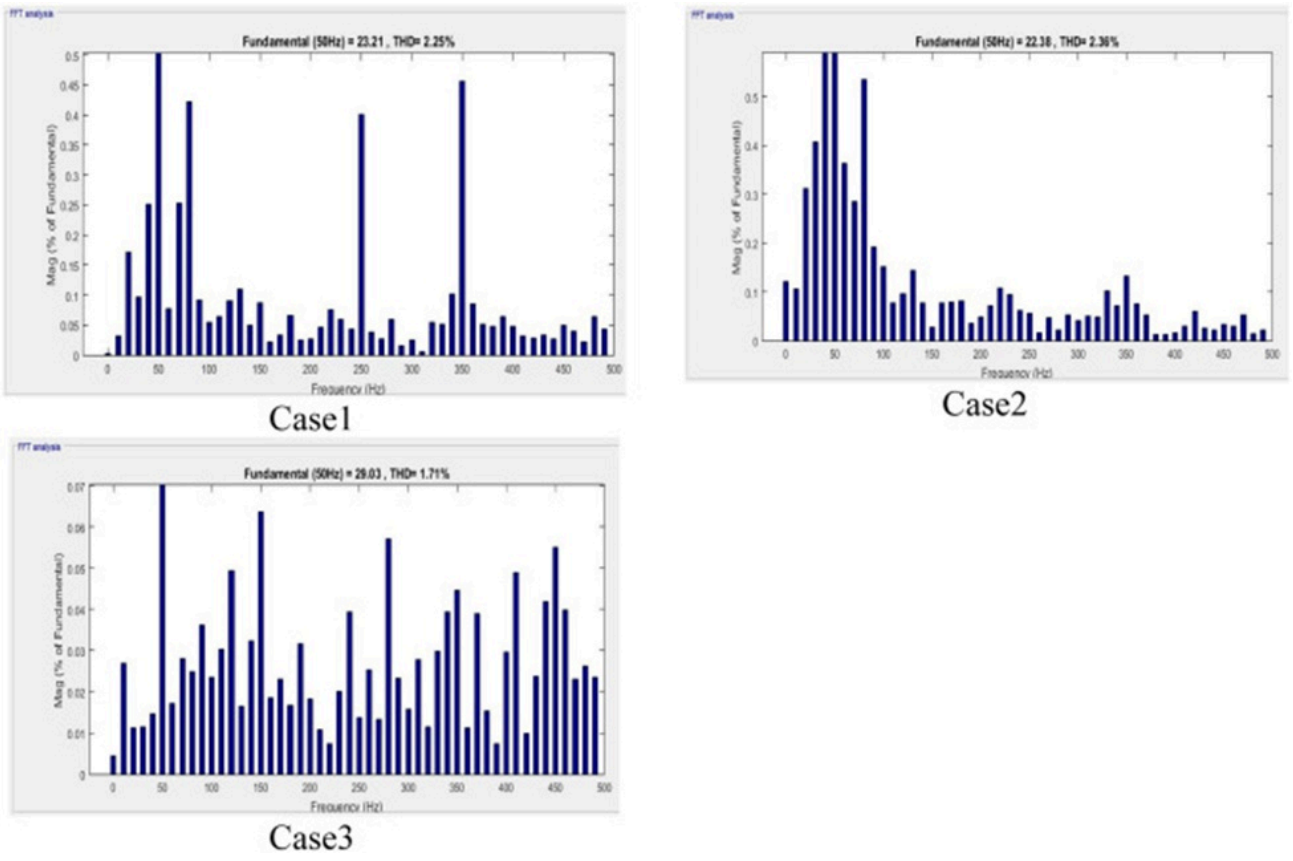
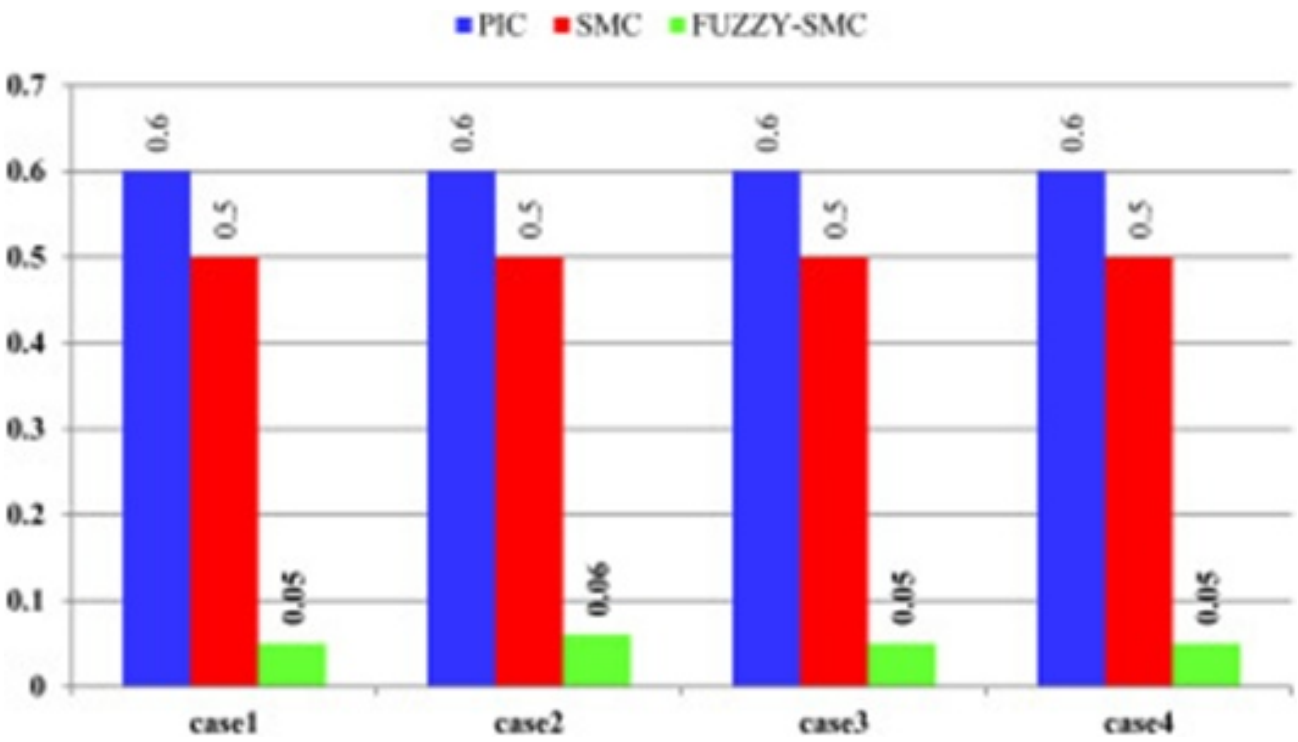


Figure 13. Spectrum of source THD



© 2024 The Author(s). | Published by Institute of Smart Energy Systems Press

Figure 14. Time taken (sec) for DC link voltage to reach stability.

Conclusion

Control strategies for the solar energy system (SES) and battery energy storage (BES) were formulated in conjunction with the FSMC applied to the UPQC's SHAF and SEAF. This integration was designed to consistently maintain a stable DC-link capacitor voltage amid fluctuating load demands and varying solar irradiance. The core objectives of this architecture involved the eradication of source voltage sags, swells, and harmonics, alongside the rectification of current waveform imperfections to drastically minimize THD. Evaluation of the proposed methodology's effectiveness across four distinct test studies confirms its robust capability to significantly reduce THD and reliably supply power to the load during islanded operations. A comparative assessment against conventional PIC, standard SMC, and additional controllers discussed in the existing literature further demonstrates that the proposed controller outperforms alternative methods. Experimental analysis across the four test studies proves the system's proficiency in reducing THD to 2.25%, 2.36%, and 1.71%, respectively. These findings definitively show that the introduced control strategy successfully manages THD within acceptable limits. Future research endeavors could focus on adapting and investigating this proposed system for multi-level UPQC applications.

Acknowledgements

None

Conflict of interest

None

Financial support

None

Ethics statement

None

Received: 24 Apr 2023 Revised: 29 Jun 2023 Accepted: 14 Jul 2023
Published online: 15 November 2024

Rights and permissions

Open Access The author(s) retain copyright. This article is licensed under the Creative Commons Attribution-NonCommercial-ShareAlike 4.0 International License. It may be shared and adapted for non-commercial purposes with appropriate attribution, an indication of changes, and distribution of adaptations under the same license. Third-party material may be subject to separate terms identified in its credit line. View the license at https://creativecommons.org/licenses/by-nc-sa/4.0/.

References

© 2024 The Author(s). | Published by Institute of Smart Energy Systems Press

1. Sai Sarita NC, Suresh Reddy S, Sujatha P. Control strategies for power quality enrichment in Distribution network using UPQC. Mater Today Proc. 2023;80:2872-82. https://doi.org/10.1016/j.matpr.2021.07.053.

2. Poongothai S, Srinath S. Power quality enhancement in solar power with grid connected system using UPQC. Microprocess Microsyst. 2020;79:103300. https://doi.org/10.1016/j.micpro.2020.103300.

3. Gowtham N, Shankar S. UPQC: a custom power device for power quality improvement. Mater Today Proc. 2018;5(1):965-72. https://doi.org/10.1016/j.matpr.2017.11.172..

4. Kumar S, Rajasekar S, Ajay-d-Vimal Raj P. Power quality profile enhancement of utility connected microgrid system using ANFIS-UPQC. Procedia Technol. 2015;21:112-9. https://doi.org/10.1016/j.protcy.2015.10.017.

5. Samal S, Hota PK. Design and analysis of solar PV-fuel cell and wind energy based microgrid system for power quality improvement. Cogent Eng. 2017;4:1-22.

6. Subanth Williams A, Suja Mani Malar R, Ahilan T. Wind connected distribution system with intelligent controller based compensators for power quality issues mitigation. Electr Power Syst Res. 2023;217:109103. https://doi.org/10.1016/j.epsr.2022.109103.

7. Renduchintala UK, Pang C, Tatikonda KM, Yang L. ANFIS-Fuzzy logic based UPQC in interconnected microgrid distribution systems: modeling, simulation and implementation. J Eng. 2021;2021:6-18. https://doi.org/10.1049/tje2.12005.

8. Pazhanimuthu C, Ramesh S. Grid integration of renewable energy sources (RES) for power quality improvement using adaptive fuzzy logic controller based series hybrid active power filter (SHAPF). J Intell Fuzzy Syst. 2018;35:749-66. https://doi.org/10.3233/JIFS-169727.

9. Sakthivel A, Vijayakumar P, Senthilkumar A, Lakshminarasimman L, Paramasivam S. Experimental investigations on ant colony optimized pi control algorithm for shunt active power filter to improve power quality. Control Eng Pract. 2015;42:153-69. https://doi.org/10.1016/j.conengprac.2015.04.013.

10. Dheeban SS, Muthu Selvan NB. ANFIS-based power quality improvement by photovoltaic integrated UPQC at distribution system. IETE J Res. 2023;69(5):2353-71. https://doi.org/10.1080/03772063.2021.1888325.

11. Krishna D, Sasikala M, Ganesh V. Adaptive FLC-based UPQC in distribution power systems for power quality problems. Int J Ambient Energy. 2022;43(1):1719-29. https://doi.org/10.1080/01430750.2020.1722232.

12. Suja KR, Raglend IJ. Adaptive genetic Algorithm/Neuro-fuzzy logic controller based unified power quality conditioner controller for compensating power quality problems. Aust J Electr Electron Eng. 2013;10(3):351-61. https://doi.org/10.7158/1448837X.2013.11464384.

13. Gandhar S, Ohri J, Singh M. A mathematical framework of ANFIS tuned UPQC controlled RES based isolated microgrid system. J Interdiscip Math. 2022;25(5):1467-77. https://doi.org/10.1080/09720502.2022.2046332.

14. Vinnakoti S, Kota VR. Performance analysis of ANN-based multilevel UPQC under faulty and overloading conditions. Int J Ambient Energy. 2021;42(13):1516-28. https://doi.org/10.1080/01430750.2019.1611645.

© 2024 The Author(s). | Published by Institute of Smart Energy Systems Press

15. Sankar JI, Subbaraman S. Multi-converter UPQC optimization for power quality improvement using beetle swarm-based butterfly optimization algorithm. Electr Power Compon Syst. 2023;51(20):2487-98. https://doi.org/10.1080/15325008.2023.2210575.

16. Yadav SK, Sabitha B, Prabhakaran A. Optimal placement of UPQC in distribution network using hybrid approach. Cybern Syst. 2023;54(7):1014-36. https://doi.org/10.1080/01969722.2022.2129378.

17. Jin J, Li H, Yang R, Li Y, Zhou Q, Feng G, et al. An improved compensation method for voltage sags and swells of the electric vehicles charging station based on a UPQC-SMES system. Int J Electr Power Energy Syst. 2022;143:108501. https://doi.org/10.1016/j.ijepes.2022.108501.

18. Golla M, Sankar S, Chandrasekaran K. Renewable integrated UAPF fed microgrid system for power quality enhancement and effective power flow management. Int J Electr Power Energy Syst. 2021;133:107301. https://doi.org/10.1016/j.ijepes.2021.107301.

19. Arulkumar T, Chandrasekaran N. Development of improved sparrow search-based PI controller for power quality enhancement using UPQC integrated with medical devices. Eng Appl Artif Intell. 2022;116:105444. https://doi.org/10.1016/j.engappai.2022.105444.

20. Senthilkumar A, Ajay-d-Vimal Raj P. ANFIS and MRAS-PI controllers based adaptive-UPQC for power quality enhancement application. Electr Power Syst Res. 2015;126:1-11. https://doi.org/10.1016/j.epsr.2015.04.013.

© 2024 The Author(s). | Published by Institute of Smart Energy Systems Press